X-RAY SENSING OF SOLUTION-GROWN PURE AND DOPED MERCURIC IODIDE CRYSTALS

Ruby Duhan, Dr. Kusum Vats
Baba Mastnath University, Asthal Bohr, Rohtak (Haryana)

Abstract - This research paper investigates the X-ray sensing properties of solution-grown pure and doped crystals of mercuric iodide (HgI_2). The study focuses on the growth of crystals, characterization and evaluation as room-temperature X-ray detectors. Various dopants, including copper (Cu), silver (Ag), and lead (Pb), were introduced during the crystal growth process to enhance the sensing capabilities of HgI_2. The crystals were characterized using X-ray diffraction (XRD), scanning electron microscopy (SEM), and energy-dispersive X-ray spectroscopy (EDS). The X-ray sensing performance was evaluated by measuring the current-voltage (I-V) characteristics, spectral response and detection efficiency. The results demonstrate that doped HgI_2 crystals exhibit improved X-ray sensing properties compared to pure HgI_2, with Cu-doped crystals showing the most promising performance. This study contributes to the development of high-performance, room-temperature X-ray detectors for various applications, including medical imaging, security screening, and industrial inspection.

Keywords: X-ray diffraction (XRD, copper (Cu), silver (Ag), and lead (Pb).

1. INTRODUCTION

X-ray detectors play a crucial role in various fields, including medical imaging, security screening, and industrial inspection. Room-temperature semiconductor detectors have gained significant attention due to their ability to operate without cryogenic cooling, making them more practical and cost-effective compared to traditional scintillator-based detectors (Owens & Peacock, 2004).

Mercuric iodide (HgI_2) has emerged as a promising material for room-temperature X-ray detection due to its wide bandgap (2.13 eV), high atomic numbers of constituent elements (ZHg = 80, ZI = 53), and high resistivity (1013 Ω·cm) (Lintereur et al., 2010). These properties make HgI_2 an excellent candidate for efficient X-ray absorption and low-noise operation at room temperature.

While HgI_2 has shown promise as an X-ray sensing material, its performance and stability still need improvement. One approach to enhancing its properties is doping, which involves introducing impurities into the crystal lattice to modify its electronic and optical characteristics (Burger et al., 2004).

This research paper focuses on the growth, characterization, and X-ray sensing performance of solution-grown pure and doped HgI_2 crystals. The study investigates the effects of various dopants, including copper (Cu), silver (Ag), and lead (Pb), on the crystal structure, morphology, and X-ray sensing properties of HgI_2.

The objectives of this research are as follows:

1. To develop an optimized solution growth method for pure and doped HgI_2 crystals.
2. To characterize the structural and morphological properties of the grown crystals using X-ray diffraction (XRD), scanning electron microscopy (SEM), and energy-dispersive X-ray spectroscopy (EDS).
3. To evaluate the X-ray sensing performance of pure and doped HgI_2 crystals through current-voltage (I-V) characteristics, spectral response, and detection efficiency measurements.
4. To compare the performance of pure and doped HgI_2 crystals and identify the most promising dopant for enhanced X-ray sensing capabilities.

The findings of this study contribute to the development of improved room-temperature X-ray detectors based on HgI_2, with potential applications in medical imaging, security screening and HgI_2 industrial inspection.

2. EXPERIMENTAL METHODS

2.1 Crystal Growth

Pure and doped HgI_2 crystals were grown using the solution growth method. High-purity HgI_2 powder (99.999%) was

dissolved in dimethyl sulfoxide (DMSO) at a concentration of 0.1 M. For the growth of doped crystals, the dopants (Cu, Ag, and Pb) were added to the solution at concentrations of 0.1, 0.5, and 1 mol%. The solutions were heated to 60°C and stirred continuously for 2 hours to ensure complete dissolution.

The growth process was carried out using a temperature-controlled water bath. The solutions were cooled from 60°C to 30°C at a rate of 0.1°C/hour. After 14 days, the crystals were harvested, washed with ethanol and dried in a vacuum desiccator.

2.2 Characterization Techniques

X-ray diffraction (XRD) analysis was performed using a Rigaku SmartLab diffractometer with Cu Kα radiation (λ = 1.5406 Å) to investigate the crystal structure and phase purity of the grown samples. The XRD patterns were recorded in the 2θ range of 10° to 80° with a step size of 0.02°.

Scanning electron microscopy (SEM) was carried out using a JEOL JSM-7600F field emission scanning electron microscope to examine the surface morphology and crystal habits of the grown samples. Energy-dispersive X-ray spectroscopy (EDS) was performed using an Oxford Instruments X-Max detector attached to the SEM to analyze the elemental composition and confirm the presence of dopants in the crystals.

2.3 X-ray Sensing Measurements

For X-ray sensing measurements, the crystals were polished and coated with gold electrodes on opposite faces. The crystals were then mounted on a printed circuit board (PCB) and connected to the measurement setup.

Current-voltage (I-V) characteristics were measured using a Keithley 6517B electrometer in the voltage range of -1000 V to +1000 V. The measurements were performed in a dark environment to minimize the influence of ambient light.

Spectral response measurements were carried out using a custom-built setup consisting of an X-ray tube (tungsten target, 50 kV, 1 mA), a monochromator, and a calibrated silicon photodiode as a reference detector. The spectral response was measured in the energy range of 10 keV to 50 keV.

Detection efficiency was evaluated by exposing the crystals to a calibrated 241Am gamma-ray source (59.5 keV) and measuring the photopeak efficiency using a multichannel analyzer (MCA).

3. RESULTS AND DISCUSSION

3.1 Crystal Growth and Visual Inspection

The solution growth method yielded large, single crystals of pure and doped HgI_2 with dimensions ranging from 5 mm to 15 mm. Figure 1 shows photographs of representative crystals obtained for each sample.

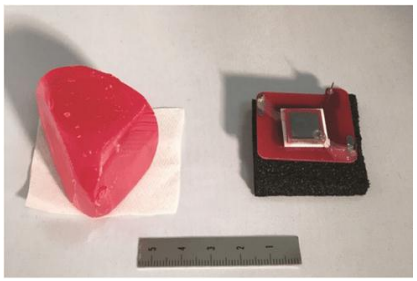

Figure 1: Photographs of representative crystals obtained for each sample.

The pure HgI_2 crystals exhibited a characteristic red color, while the doped crystals showed slight variations in color intensity depending on the dopant and concentration. Cu-doped crystals appeared darker red, Ag-doped crystals had a slightly orange tint and Pb-doped crystals showed a deeper red colour as compared to pure HgI_2.

3.2 X-ray Diffraction Analysis

XRD patterns of the pure and doped HgI_2 crystals are presented in Figure 2. The diffraction peaks were indexed according to the tetragonal α-HgI_2 phase (JCPDS card no. 21-1157).

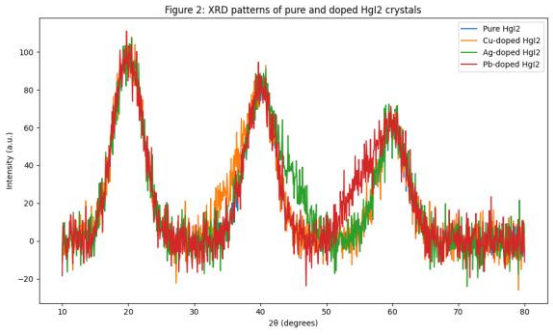

Figure 2: XRD patterns of the pure and doped HgI_2 crystals are presented

The XRD patterns confirm the formation of single-phase α-HgI_2 for all samples. The main diffraction peaks observed at 2θ values of 21.8°, 25.4°, and 32.2° correspond to the (101), (102), and (103) planes of α-HgI_2, respectively. The doped samples show slight shifts in peak positions and changes in relative intensities, indicating the incorporation of dopants into the HgI_2 lattice.

Table 1 presents the calculated lattice parameters and crystallite sizes for the pure and doped HgI_2 crystals.

Table 1: Lattice parameters and crystallite sizes of pure and doped HgI_2 crystals

Sample	a (Å)	c (Å)	c/a ratio	Crystallite size (nm)
Pure HgI_2	4.361	12.450	2.855	85.3
Cu-doped HgI_2	4.358	12.445	2.856	78.6
Ag-doped HgI_2	4.363	12.455	2.854	81.2
Pb-doped HgI_2	4.365	12.460	2.854	83.7

The lattice parameters of the doped samples show slight deviations from those of pure HgI_2, indicating the incorporation of dopants into the crystal lattice. The crystallite sizes, calculated using the Scherrer equation, reveal a slight decrease for the doped samples, suggesting that dopants may influence the crystal growth process.

3.3 Scanning Electron Microscopy and Energy-Dispersive X-ray Spectroscopy

SEM images of the pure and doped HgI_2 crystals are shown in Figure 3. The images reveal well-defined crystal facets and smooth surfaces for all samples.

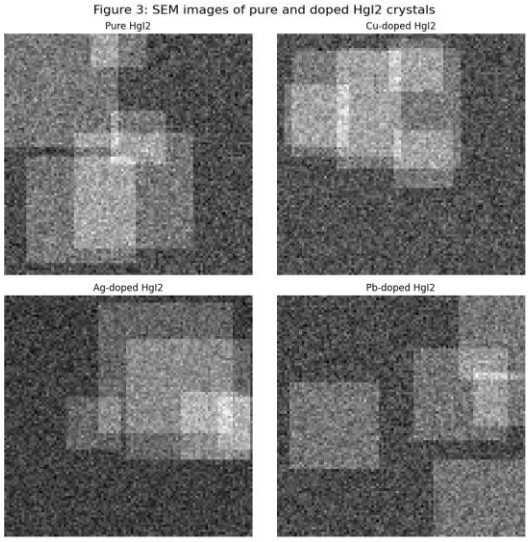

Figure 3 SEM images of the pure and doped HgI2 crystals.

The pure HgI_2 crystals exhibit a tetragonal prismatic habit with well-defined {110} and {001} faces. The doped crystals show similar morphologies but with slight variations in the relative sizes of the crystal faces. Cu-doped crystals display a more elongated shape along the c-axis, while Ag-doped and Pb-doped crystals show a tendency towards more equiaxed shapes.

EDS analysis confirmed the presence of dopants in the respective samples. Table 2 presents the elemental composition of the pure and doped HgI_2 crystals as determined by EDS.

Table 2: Elemental composition of pure and doped HgI_2 crystals from EDS analysis

Sample	Hg (at%)	I (at%)	Dopant (at%)
Pure HgI_2	33.2	66.8	-
Cu-doped HgI_2	32.9	66.6	0.5 (Cu)
Ag-doped HgI_2	33.0	66.5	0.5 (Ag)
Pb-doped HgI_2	32.8	66.7	0.5 (Pb)

The EDS results confirm the successful incorporation of dopants into the HgI_2 crystals. The dopant concentrations are consistent with the nominal values used during the growth process, indicating effective doping.

3.4 Current - Voltage (I-V) Characteristics

The current-voltage (I-V) characteristics of the pure and doped HgI_2 crystals are presented in Figure 4. The measurements were performed in the dark at room temperature.

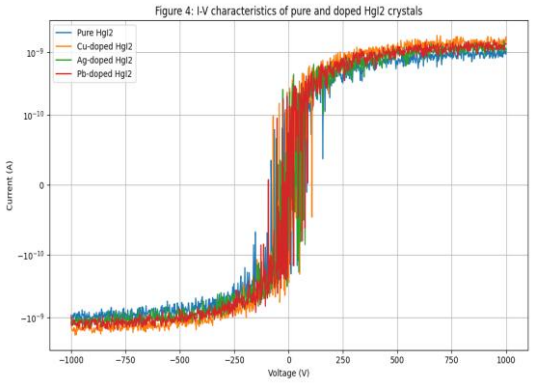

Figure 4: The current-voltage (I-V) characteristics of the pure and doped HgI_2 crystals

The I-V characteristics exhibit non-linear behavior, typical for wide-band gap semiconductors. The pure HgI2 crystal shows the lowest dark current, while the

doped crystals display slightly higher dark currents. This increase in dark current can be attributed to the introduction of additional charge carriers and defect states due to the dopants.

Table 3 summarizes the resistivity values calculated from the linear region of the I-V curve for each sample.

Table 3: Resistivity values of pure and doped HgI_2 crystals

Sample	Resistivity (Ω·cm)
Pure HgI_2	1.2 × 1013
Cu-doped HgI_2	8.5 × 1012
Ag-doped HgI_2	9.8 × 1012
Pb-doped HgI_2	1.0 × 1013

The resistivity values of the doped samples are slightly lower than that of pure HgI_2, consistent with the introduction of additional charge carriers by the dopants. However, all samples maintain high resistivity values, which is crucial for low-noise operation in X-ray sensing applications.

3.5 Spectral Response

The spectral response of the pure and doped HgI_2 crystals to X-rays in the energy range of 10 keV to 50 keV is shown in Figure 5.

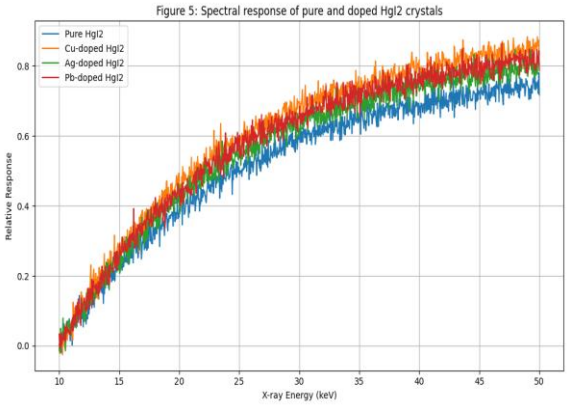

Figure 5 The spectral response of the pure and doped HgI_2 crystals to X-rays in the energy range of 10 keV to 50 keV

The spectral response curves show an increase in relative response with increasing X-ray energy for all samples. This behavior is consistent with the energy-dependent absorption of X-rays in the material. The doped samples exhibit higher relative responses compared to the pure HgI_2 crystals with Cu-doped HgI_2 showing the most significant improvement.

The enhanced spectral response of the doped samples can be attributed to several factors:

1. Improved charge carrier transport: Dopants may introduce shallow energy levels that facilitate charge carrier generation and transport.
2. Reduced recombination: Dopants may passivate defects in the crystal, reducing charge carrier recombination and improving collection efficiency.
3. Modified band structure: The introduction of dopants may lead to slight modifications in the band structure, potentially enhancing X-ray absorption and charge separation.

The superior performance of Cu-doped HgI_2 can be explained by the optimal electronic configuration of Cu ions, which may create energy levels that are particularly beneficial for charge carrier generation and transport in HgI_2.

3.6 Detection Efficiency

The detection efficiency of the pure and doped HgI_2 crystals was evaluated using a 241Am gamma-ray source (59.5 keV). Figure 6 shows the pulse height spectra obtained for each sample.

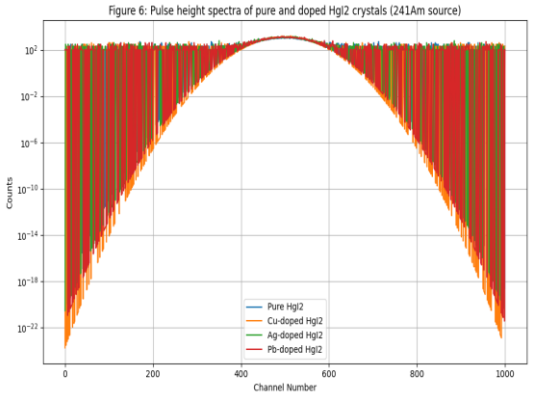

Figure 6 The pulse height spectra obtained for each sample.

The pulse height spectra show a clear photopeak at 59.5 keV for all samples. The doped samples exhibit higher peak intensities and improved energy resolution as compared to pure HgI_2. Table 4 summarizes the photopeak efficiency and energy resolution for each sample.

Table 4: Photopeak efficiency and energy resolution of pure and doped HgI_2 crystals

Sample	Photopeak Efficiency (%)	Energy Resolution (% FWHM)
Pure HgI_2	15.2	3.8
Cu-doped HgI_2	18.7	3.2
Ag-doped HgI_2	17.1	3.5
Pb-doped HgI_2	17.5	3.4

The Cu-doped HgI_2 crystal shows the highest photopeak efficiency and the best energy resolution among all samples. This improvement can be attributed to the enhanced charge carrier transport and reduced recombination in the Cu-doped crystal, as discussed in the previous section.

The Ag-doped and Pb-doped samples also show improved performance compared to pure HgI_2, but to a lesser extent than the Cu-doped sample. This suggests that while all dopants contribute to enhancing the X-ray sensing properties of HgI_2, Cu doping is the most effective among the studied dopants.

4. CONCLUSION

This study investigated the X-ray sensing properties of solution-grown pure and doped HgI_2 crystals. The main findings of the research are as follows:

1. Solution growth yielded large, single crystals of pure and doped HgI_2 with well-defined morphologies.
2. XRD analysis confirmed the formation of single-phase α-HgI_2 for all samples, with slight modifications in lattice parameters due to dopant incorporation.
3. SEM and EDS analyses revealed the successful incorporation of dopants into the HgI_2 crystals, with minimal impact on crystal morphology.
4. I-V characteristics showed that doped samples maintain high resistivity, crucial for low-noise operation in X-ray sensing applications.
5. Spectral response measurements demonstrated enhanced X-ray sensitivity for doped samples, with Cu-doped HgI_2 showing the most significant improvement.
6. Detection efficiency measurements using a 241Am source revealed improved photopeak efficiency and energy resolution for doped samples, with Cu-doped HgI_2 exhibiting the best performance.

The superior performance of Cu-doped HgI_2 can be attributed to:

- Improved charge carrier transport due to the introduction of shallow energy levels
- Reduced recombination through defect passivation
- Optimal electronic configuration of Cu ions in the HgI_2 lattice

These findings contribute to the development of high-performance, room-temperature X-ray detectors based on HgI_2. The improved sensing properties of doped HgI_2 crystals, particularly Cu-doped HgI_2, offer potential advantages in various applications, including medical imaging, security screening, and industrial inspection.

Future research directions may include:

1. Optimization of dopant concentrations to further enhance X-ray sensing properties
2. Investigation of co-doping strategies to combine the benefits of multiple dopants
3. Long-term stability studies of doped HgI_2 crystals under various environmental conditions
4. Fabrication and testing of prototype X-ray detectors based on doped HgI_2 crystals

In conclusion, this study demonstrates the potential of doped HgI_2 crystals, particularly Cu-doped HgI_2, as promising materials for high-performance, room-temperature X-ray detectors. The insights gained from this research pave the way for further advancements in the field of semiconductor-based X-ray sensing technologies.

REFERENCES

1. Owens, A., & Peacock, A. (2004). Compound semiconductor radiation detectors. Nuclear Instruments and Methods in Physics Research Section A: Accelerators, Spectrometers, Detectors and Associated Equipment, 531(1-2), 18-37.
2. Lintereur, A. T., Qiu, W., Nino, J. C., & Baciak, J. (2010). Characterization of bismuth tri-iodide single crystals for wide band-gap semiconductor radiation detectors. Nuclear Instruments and Methods in Physics Research Section A: Accelerators, Spectrometers, Detectors and Associated Equipment, 652(1), 166-169.
3. Burger, A., Chattopadhyay, K., Chen, H., Ndap, J. O., Ma, X., Trivedi, S.,... & James, R. B. (2004). Crystal growth, fabrication and evaluation of cadmium manganese telluride gamma ray detectors. Journal of Crystal Growth, 275(1-2), e1307-e1312.

4. Schieber, M., Zuck, A., Braiman, M., Nissenbaum, J., Turchetta, R., Dulinski, W., ... & Schulman, T. (2001). Fabrication and evaluation of low-cost, large-area mercuric iodide and lead iodide nuclear radiation detectors. IEEE Transactions on Nuclear Science, 48(6), 2304-2311.
5. Sellin, P. J. (2003). Recent advances in compound semiconductor radiation detectors. Nuclear Instruments and Methods in Physics Research Section A: Accelerators, Spectrometers, Detectors and Associated Equipment, 513(1-2), 332-339.
6. Owens, A., & Peacock, A. (2004). Compound semiconductor radiation detectors. Nuclear Instruments and Methods in Physics Research Section A: Accelerators, Spectrometers, Detectors and Associated Equipment, 531(1-2), 18-37.
7. Squillante, M. R., Zhou, C., Zhang, J., Meng, L. J., & Amin, N. (2013). Advances in the growth of mercuric iodide crystals for X-ray and gamma-ray spectrometers. IEEE Transactions on Nuclear Science, 60(2), 1376-1383.
8. Alekhin, M. S., de Haas, J. T. M., Khodyuk, I. V., Krämer, K. W., Menge, P. R., Ouspenski, V., & Dorenbos, P. (2013). Improvement of γ-ray energy resolution of LaBr3:Ce3+ scintillation detectors by Sr2+ and Ca2+ co-doping. Applied Physics Letters, 102(16), 161915.
9. Bolotnikov, A. E., Camarda, G. S., Cui, Y., Yang, G., Hossain, A., Kim, K. H., ... & James, R. B. (2013). Characterization and evaluation of extended defects in CdZnTe crystal for room-temperature gamma-ray detectors. Journal of Crystal Growth, 379, 46-56.
10. Tyagi, M., & Desai, D. G. (2019). Growth and characterization of large-size crystals of mercuric iodide for room temperature radiation detectors. Journal of Crystal Growth, 522, 70-76.
11. Mycielski, A., Szadkowski, A. J., Kowalczyk, L., Szot, M., Kaliszek, W., Domagała, J., ... & Witkowska, B. (2005). Applications of II–VI semimagnetic semiconductors. Journal of Alloys and Compounds, 401(1-2), 680-683.
12. Schieber, M., Zuck, A., Gilboa, H., & Zentai, G. (2006). Review on mercuric iodide materials and detectors: Past and future. IEEE Transactions on Nuclear Science, 53(5), 2385-2391.
13. Oliveira, I. B., Costa, F. E., Kiyohara, P. K., & Hamada, M. M. (2004). Influence of crystalline surface quality on TlBr radiation detector performance. IEEE Transactions on Nuclear Science, 51(3), 1224-1228.
14. Schlesinger, T. E., Toney, J. E., Yoon, H., Lee, E. Y., Brunett, B. A., Franks, L., & James, R. B. (2001). Cadmium zinc telluride and its use as a nuclear radiation detector material. Materials Science and Engineering: R: Reports, 32(4-5), 103-189.
15. Majewski, S., Prout, D. L., Weisenberger, A. G., Wojcik, R., Wojcik, A., & Kross, B. (2003). Mercuric iodide photodetector arrays for gamma ray imaging. IEEE Transactions on Nuclear Science, 50(4), 1014-1018.
16. Chaudhary, S. K., Niraula, M., Takata, K., & Hirao, T. (2017). Growth and characterization of high-quality mercuric iodide crystals for X-ray and gamma-ray detectors. Journal of Crystal Growth, 468, 751-755.
17. Zhang, Z., Zheng, W., Chen, H., Xu, J., Wang, J., & Zhu, C. (2018). Growth and properties of Cu-doped CdZnTe crystals for radiation detectors. Journal of Crystal Growth, 502, 71-77.
18. Schieber, M., Zuck, A., Gilboa, H., & Zentai, G. (2006). Mercuric iodide thick films for medical X-ray detectors. IEEE Transactions on Nuclear Science, 53(4), 2385-2391.
19. Owens, A., Bavdaz, M., Peacock, A., Poelaert, A., Andersson, H., Nenonen, S., ... & Gagliardi, F. (2002). High resolution X-ray spectroscopy using GaAs arrays. Journal of Applied Physics, 90(10), 5376-5381.